Horizontal humidity gradient from one single scanning microwave radiometer

Jan H. Schween, S. Crewell, *member, IEEE*, U. Löhnert,

***Abstract*—We present a method for deriving horizontal humidity variability from a single scanning passive microwave radiometer. The microwave radiometer used has full scanning capabilities in azimuth and elevation and is sensitive to the path integrated water vapor as well as cloud liquid water. Applying a simple linear gradient model together with an assumed vertical profile derived from the closest radiosonde ascent, the strength and direction of the horizontal humidity gradient can be determined with a temporal resolution on the order of 15-20 minutes. For the case of an approaching frontal system the derived humidity field can explain up to 88% of the measured humidity variance - the missing variance can most probably be attributed to convective activity.**

I. Introduction

In order to accurately characterize and ultimately simulate convective activity, knowledge of the three-dimensional structure and temporal development of the pre-convective environment is necessary. Especially important is capturing water vapor variability on small scales (1 m to 10 km) and no suitable operational measurement technique exists as of today. Radiosoundings giving high vertical resolution can not describe horizontal gradients on the local scale. Polar orbiting satellites with sensors operating in the visible spectrum (e.g. Medium Resolution Imaging Spectrometer Instrument, MERIS onboard the European Space Agency Environmental Satellite, ENVISAT) can derive integrated water vapor (IWV) [1] with high spatial resolution (up to 260 m). However, they are limited to overpass times and cloud-free situations. High repetition time can be gained from geostationary satellites but measurements are limited to several kilometers resolution and the upper troposphere. Additionally, no satellite sensor has the potential of deriving information of boundary layer water vapor structures.

From the ground-based point of view, some remote sensing methods exist which have the potential of describing the water vapor field on the scales mentioned above. Raman lidar and differential absorption lidar (DIAL) technologies are still on the advent of becoming suited for routine operational measurements. First scanning DIAL measurements have nicely shown the potential for deriving 3-dimensional water vapor within an area of 2-3 km around the measurement site [2]. Global Positioning System (GPS) observations are widely used to determine the wet zenith path delay which is, in general, directly proportional to IWV. While the standard approach includes delay measurements between the ground station and several GPS satellites, it is also possible to retrieve IWV along the line of sight to a single satellite [3], however, the observations are random in space and time due to satellite configurations.

Passive microwave technology is well suited for determining IWV variations in time and observing direction as could be demonstrated by [4] using an airborne comparison. Additionally, passive microwave radiometers (MWR) have proven to be suitable for long-term, uninterrupted and automatic measurements in the last 10 years. Padmanabhan et al. 2009 [5] have shown first results with 500 m resolution on a 10 km scale for deriving three-dimensional water vapor structures for a triangular set-up of three identical water vapor sensitive MWRs. Simulation studies show errors on the order of 20-30% under the pre-condition of a close-by sounding which provides an a priori profile as constraint. Schneebeli [6] used data from a scanning microwave radiometer and analysed it using empirical orthogonal functions. He could show that during frontal passages the direction of the main variation in the IWV field has the same direction as the wind at the surface.

This study outlines a model for a single MWR in continuous volume scanning mode to derive the strength and direction of horizontal water vapor density gradients (section II) in conjunction with a priori information derived from a close-by radiosonde. A similar approach was taken by [7], who showed the importance of using scanning measurements of a single MWR for determining local gradients of wet path delay for radio-interferometric geodetic studies. They applied a linear model to MWR data, which was later used by [8] to perform a statistical analysis of wet path delay gradients at a Swedish station.

The measurement configuration of the study presented here is - in contrast to the multi-instrument tomographic setup of [5] - fairly simple and delivers automatically, continuously running volume scans (section III). For one particular day with a strong IWV increase of more than 20 kgm^{-2} (section IV) the described model is applied to characterize the small-scale temporal development of the spatial IWV gradient (section V). Section VI summarizes the results and proposes the further development of the applied model.

II. Method

Integrated water vapor (IWV) abbreviated here as $\widetilde{W}$ for a slanted column, is the integral over water vapor density ρ_v

Manuscript received August 29, 2010; revised sometimes later

This work was financially supported by the Transregional collaborative research centre (SFB/TR 32) 'Pattern in Soil-Vegetation-Atmosphere Systems: Monitoring, Modelling, and Data Assimilation' funded by the Deutsche Forschungsgemeinschaft (DFG).

J.H. Schween, S. Crewell, U. Löhnert are with Institute for Geophysics and Meteorology, University of Cologne, Germany

Email: jschween@uni-koeln.de

along a line of sight:

$$\widetilde{W} = \int_0^\infty \rho_v(r)\ dr \tag{1}$$

with r the distance along the line of sight. We are interested in how an inhomogeneous water vapor field $\rho_v(x, y, z)$ appears in measured $\widetilde{W}$-values with the radiometer positioned at $x = y = z = 0$. As a first order linear approach we assume that a horizontal gradient exists only in x-direction with the x-axis aligned in the direction of the gradient. Then the water vapor density at the surface (z=0) is given by:

$$\rho_{v0}(x) = A_0 + A_1 \cdot x \tag{2}$$

with A_0 the vertical average boundary layer water vapor density at the radiometer position and A_1 the horizontal gradient in mass per volume and distance. Note, that this equation is only applicable in a limited range away from the radiometer as no saturation or negative values of humidity are reached. For the vertical coordinate we assume a constant value in the boundary layer ($z \leq h$) and an exponential decay in the free troposphere above:

$$\rho_v(x, z) = \begin{cases} \rho_{v0}(x) & z \leq h \\ \rho_{v0}(x) \cdot \exp\left(-\frac{z-h}{L}\right) & z > h \end{cases} \tag{3}$$

With this model we assume that humidity variation in the horizontal is only determined by the gradient in ρ_v while parameters h and L are assumed to be constant. This is a crude simplification but seems to be justified as we only consider an area of a few couple of kilometers and a more general model would incorporate too many degrees of freedom to get reliable results. The profile in the free troposphere is connected to the boundary layer but the gradient here is by a factor $\exp(-(z-h)/L)$ smaller than in the boundary layer. This profile form is a pragmatic approach to keep calculations simple: In a well mixed boundary layer, the water vapor mass mixing ratio μ should be constant rather than ρ_v. As ρ_v is the product of μ and the density of air, it would decrease with height. At the top of a 1000 m well mixed boundary layer with μ =const. ρ_v will be smaller by about 20% than at the surface. Because water vapor can be very variable in the boundary layer and deviations from μ =const. are common we assume that ρ_v = const. is an acceptable simplification.

Ignoring Earth curvature, coordinates x and z are related to range r via spherical coordinates:

$$\begin{aligned} x &= r \cdot \sin\theta \cdot \cos\alpha \\ z &= r \cdot \cos\theta \end{aligned} \tag{4}$$

with zenith angle θ and azimuth angle α. After replacing variables x and z in (3), ρ_v is inserted into (1) and integrated. In order to correct for the relative optical airmass, we multiply with $\cos\theta$ and define $W = \widetilde{W} \cdot \cos\theta$ as the airmass corrected water vapor column. So far we assume a gradient in x-direction. If the direction is different this is equivalent to a rotation of the coordinate system and will lead to a phase shift angle ϕ representing a change in the orientation of the gradient:

$$W = W_1 \cdot \tan\theta \cdot \cos(\alpha - \phi) + W_0 \tag{5}$$

In other words the airmass corrected integrated water vapor W as a function of azimuth angle is a cosine wave. Despite the correction for the relative airmass, the amplitude of the cosine still depends on the zenith angle via $\tan\theta$. This is due to the fact that with increasing zenith angle the horizontal gradient has a stronger impact on W than close to the zenith direction. This equation is nearly identical to the equation found by [7] for the wet delay but in contrast to them we can relate the amplitude W_1 to the spatial gradient A_1 of the water vapor density field.

The offset of the cosine wave

$$W_0 = A_0 \cdot (h + L) \tag{6}$$

corresponds to the vertical column above the instrument site (zenith IWV). $A_0 h$ is the water vapor content of the boundary layer and $A_0 L$ is the content of the atmosphere above. The factor $q = h/L$ gives the ratio of the water vapor in both parts of the atmosphere. The amplitude factor is

$$W_1 = A_1 \cdot \left(\frac{1}{2}h^2 + Lh + L^2\right) \tag{7}$$

It depends not only on the gradient but also on the parameters h and L describing the shape of the water vapor profile. Parameters W_1, W_0 and ϕ can be determined by means of a least square fit to data from a scanning microwave radiometer. In our feasibility study parameters h and A_0 are determined from available radio soundings and L is derived from the zenith $\widetilde{W}$ of the radiometer by use of (6). Together they allow the calculation of the horizontal gradient A_1 of water vapor density in the boundary layer. The ultimate goal is to parameterize humidity profile shape from MWR observations alone.

III. Instrumentation and Observations

In this study we present data from September 9, 2009 measured at the research center Jülich, Germany (50^{o}54'31"N, 6^{o}24'49"E, 93m ASL) in a flat region with intensive agriculture. Integrated water vapor column values have been determined with a Humidity And Temperature PROfiler (HATPRO) microwave radiometer [9]. It measures the brightness temperatures at seven channels along the 22.235 GHz emission line of water vapor. Due to interference with surrounding microwave link networks only three channels (23.84, 27.84 and 31.4 GHz) were undisturbed and thus direct humidity profiling could not be performed. However, this frequency configuration with one channel along the wing of the water vapor line where the weighting function is roughly constant with height and two window channels is still superior to conventional 2-channel water vapor radiometers. To get slant path IWV from the observed brightness temperatures we derived, following [10], for every zenith angle a different retrieval. The absolute accuracy of derived IWV values is 1 kgm^{-2} while the precision is 0.25 kgm^{-2}.

HATPRO scans the whole upper hemisphere every 18 minutes in steps of 10^o(azimuth) and 9.6^o(zenith). At each position the measurement takes one second, a whole scan takes about 8.25 minutes and consists of 360 measuring positions. The

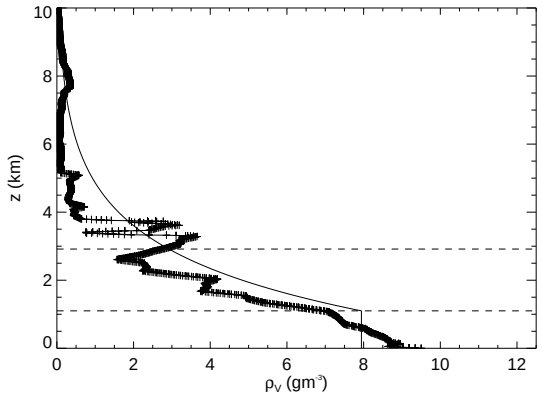

Fig. 1. Radiosonde profile from 11:17–13:05 UTC (+ signs) together with the fitted profile (solid line), boundary layer height h and scaling length for exponential decay in the free tropopshere indicated as $h + L$ (dashed lines).

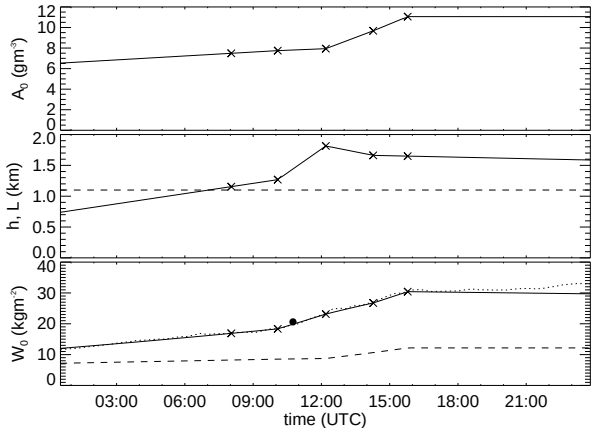

Fig. 2. Derived profile parameters for the radiosonde times ($\times$ symbol) and interpolation (lines) with: A_0 (top), h and L (middle, dashed and solid line) and resulting vertical water vapor column W_0 (bottom) recalculated from the parameters above (solid line) together with measurements from the radiometer (dotted line). The lowermost dashed line is the water vapor content of the boundary layer. The black circle at 10:45 UTC indicates the water vapor column above the site from the MERIS instrument.

antenna first points to south with low elevation (zenith angle 86.4^o), moves step by step to zenith direction, then the azimuth angle is increased by one step (10^o) to the East and the elevation mirror moves back to the horizon. This pattern is continued until the full hemisphere has been observed. As we assumed in 4 a plan parallel atmosphere, we use for this study only measurements with zenith angles smaller than 77^o. Five radiosondes (Graw DFM06) were launched between 8 and 17 UTC from a site about 6 km south of the HATPRO instrument.

IV. Environmental conditions

A. Weather situation

September 9, 2009 was characterized by an occluding front slowly approaching from the north-west. At 00 UTC it was stretching from the southern coast of Great Britain to the north-east lying 200 km away from the measuring site, however, only passing it in the early morning of the following day. The day was cloud free until around 12 UTC when thin cirrus and cirrocumulus clouds started to indicate the approach of the front. Around 15 UTC, altocumulus clouds began to cover the sky. Temperatures at 2 m height reached 27^{o}C and remained above 25^{o}C until 15:30 UTC. Wind speeds at 2 m increased during the day from nearly zero to 4 ms^{-1} in the afternoon. In the lower boundary layer (below 400 m), measurements by a nearby SODAR show weak winds below 2 ms^{-1} with no clear direction until 12 UTC when winds turned from north-west to north and increased to 5 ms^{-1} at 16 UTC. HATPRO shows a continuous increase of the vertical water vapor column W_0 from 11 kgm^{-2} (00 UTC) to 31 kgm^{-2} (16 UTC) indicating the advection of moist air ahead of the front (see also Fig.2.

B. Profile parameters

Profiles of potential temperature and dew point from the radiosoundings indicate a fairly constant boundary layer height of $h = 1100$ m during the day. This is confirmed by profiles of the aerosol backscatter coefficient from a nearby ceilometer. Water vapor density A_0 within the boundary layer is calculated as the average below h for every of the five radiosoundings of the day. The scaling length L in the free troposphere is determined from the zenith measurements of the radiometer $\widetilde{W_0}$ following (6) as $L = \widetilde{W_0}/A_0 - h$. Exemplarily, the radiosonde data from 11:17 UTC together with the fitted profile is illustrated in Fig.1. During the day the height of the boundary layer coincides with a strong vertical humidity gradient at that level confirming its position. The decrease in the free troposphere just above the boundary layer is stronger than assumed by the model, but is compensated by the humid layer around 3.5 km. This layer was visible in all profiles during the day. As ρ_V decreases in the boundary layer stronger than one would expect from theory, we tested the effect of omitting the boundary layer in the fitted profile shape (3). If only an exponential decay is considered the root mean square error (RMSE) increases for all radiosonde profiles of the day by 0.2%–31%.

The radiosonde IWV in Fig.1 is by 4 kgm^{-2} lower than the radiometer W_0 (23 kgm^{-2}) which is the largest deviation we found on that day. The radiosondes drifted with the wind in south easterly direction reaching distances of about 4.5 km at 5 km height. As this direction is opposite to the water vapor gradient, the sondes experienced a dryer airmass than the radiometer in its local zenith. For this reason, we prefer to use the zenith IWV from the radiometer rather than the radiosonde IWV for the determination of L.

Profile parameters were derived for all five radiosondes of the day and interpolated to the times of the HATPRO scans (see Fig.2). The observed increase of the water vapor is due to two effects: a rise of the water vapor density in the boundary layer A_0 mainly between 12 UTC and 16 UTC and an increase in the free troposphere above, visible in a strong rise of L between 10 UTC and 12 UTC. As h/L represents the ratio of the water vapor columns in boundary layer and free troposphere, we can conclude that the water vapor advection begins in the free troposphere, whereas the increase in the boundary layer starts after 12 UTC. This pattern can also

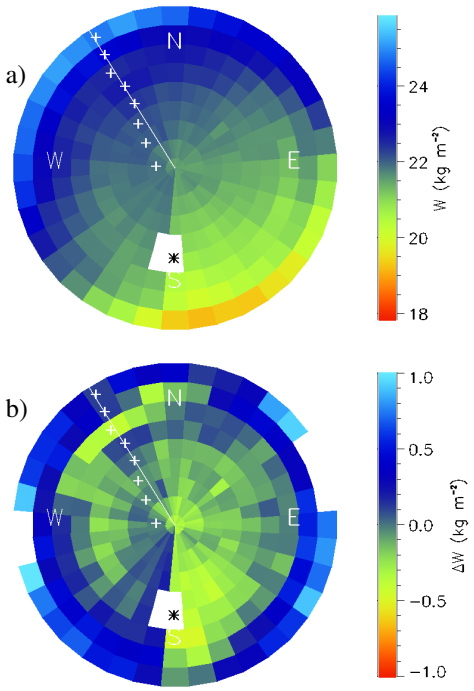

Fig. 3. Distribution of airmass corrected W for the scan of the HATPRO microwave radiometer from 11:30-11:38 UTC (a) and residuum of the fit to the whole scan (b). Zenith angle of the outermost ring is 76.8^o. The asterisk ($*$) indicates the position of the sun, plus signs ($+$) indicate the gradient direction inferred from single θ fits at the respective zenith angle and the radial line indicates the direction of the gradient from the whole scan fit.

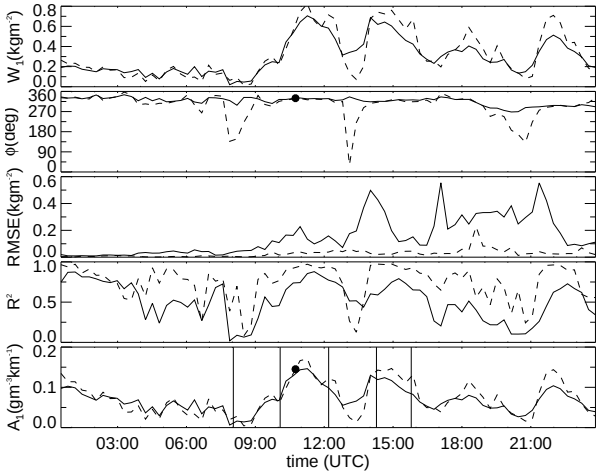

Fig. 4. Derived parameters from the HATPRO scan data for the whole scan (solid line) and for $\theta = 57.6^o$ (dashed line). From top to bottom: Amplitude W_1 of the cosine wave (5), direction ϕ of the gradient, measures for the fit quality, root mean square error of the model (RMSE) and explained variance (R^2) and calculated gradient A_1. Vertical lines in the lowermost plot indicate times of radiosonde launches. The symbol at 10:48 UTC in the ϕ and A_1 plot mark the gradient derived from MERIS data.

be seen in the W_0 values calculated from the interpolated parameters A_0, h and L. Before 12 UTC, there is no significant rise in the water vapor column of the boundary layer while the total water vapor column and the water column of the free troposphere are already rising.

V. RESULTS

A. *Water vapor scans*

Fitting equation (5) to volume scans reveals a similar structure with highest W values in the north-west, indicating that the approaching front was associated with a more humid air mass. For example, the scan from 11:30 UTC shows values between 19 kgm^{-2} and 25 kgm^{-2} at the largest zenith angle $\theta = 76.8^o$ and 21 kgm^{-2} and 23 kgm^{-2} at $\theta = 57.6^o$ giving amplitudes of 6 kgm^{-2} and 2 kgm^{-2} at the respective zenith angles. The residuum shows much smaller values between -0.5kgm^{-2} and $+1$kgm^{-2} indicating that the gradient is the dominant structure in the observed W-field. As the range of the residuum is higher than the instrument precision we can conclude that the remaining variability is not instrumental noise. Beside the fit to the whole scan, the cosine wave was fitted to every zenith angle, i.e. to every ring in Fig.3a. The resulting gradient directions ϕ of about 320^o(NW) do not differ by more than 5^o(for zenith angles larger than 20^o) supporting the assumption of a linear horizontal gradient. At the largest zenith angle (76.8^o, i.e. the outermost ring in Fig.3) W exhibits at every azimuth angle a positive bias. Considering the beam width the upper and lower part of the field of view reach h at a distance of 3.6 km and 6.4 km, respectively, this bias might arise from beam width effects in combination with atmospheric refraction.

The second dominant structure visible in the residuum (Fig.3b) is a pronounced jump between two successive azimuth angles in the south with lower values to the east and higher values to west. This is caused by a temporal change in the field during the scan, which starts at south and runs counterclockwise over east, north and west back to south. During the first minute of the scan (i.e. the first four azimuth steps) a significant increase in water vapor occurred. Afterwards the pattern follows the cosine wave fairly well, indicating that no further significant temporal change occurred. Linear detrending of the data reduced the agreement between model and scan. Patterns like this are common and it appears that a linear temporal detrending, as proposed by [7], is not sufficient to remove these artifacts.

In order to identify additional patterns Fourier analysis of scan rings at constant zenith angles was performed. No significant amplitudes could be identified in the second and third fourier component. These components would be connected to second and third components in a Taylor-expansion of the horizontal humidity field as a function of horizontal distance and would represent large scale structures. As they do not exist in the studied case, smaller convective plumes in the boundary layer appear to be responsible for the remaining fluctuations. Furhter visual insepction of the remaining structures in the residuum showed wide variation but no clear permanent pattern during the day.

B. *Derived gradients*

The derived profile parameters and scan amplitudes are combined to calculate the spatial gradient of the water vapor field by solving (7) for A_1 (Fig.4). The gradient rises up

to its day maximum of 0.14 $gm^{-3}km^{-1}$ at 11 UTC which coincides with the strongest increase of water vapor in the free troposphere (Fig.2). The second maximum around 14 UTC coincides with the strongest increase of A_0 in the boundary layer.

In order to evaluate the quality of the derived gradients with an independent method, data from the MERIS instrument [1] are suitable due to their fine spatial resolution of up to 260 m. Water vapor columns from the overpass at 10:48 UTC were used to derive the gradient in W_0 from differences over 8 km. Division by $h + L$ gives the gradient A_1 of the water vapor concentration (Fig.4). The agreement both for direction and value is nearly perfect with deviations of less than 5%.

For all 79 scans of the day the model (5) was fitted either to the whole scan or to the data from a single zenith angle $\theta = 57.6^o$ (Fig.4). The amplitude W_1 for the whole scan and for the single-θ fit agree very well most of the time, indicating that the whole field on that day is sufficiently described by the linear gradient model. This is also supported by the explained variance R^2, which reaches values of up to 88% for the whole scan. However, there are deviations between the whole scan and the single-θ fit. They are connected to low R^2 values for either of the models i.e. when the variance in the water vapor field cannot be described with the model. RMSE of the fit to the whole field is always larger than the single-θ fit. This is mainly due to the larger amplitude observed at the lowest elevation which cannot be adequately described by the model and needs to be explored.

The gradient direction ϕ is nearly constant at north-west until 18 UTC when it turns to west-north-west. There is good agreement between the whole-scan-fit and the single-θ-fit except for the times with low R^2.

VI. Summary / conclusion

The present study has shown the potential of a single full scanning MWR for detecting horizontal water vapor variability. A summer day with strong horizontal advection of water vapor was chosen to test our model. A simplified assumption of the humidity profiles (based on three parameters: A_0, h and L) together with a linear horizontal water vapor gradient (A_1) model were used to derive A_1 as well as the gradient direction (ϕ). The data revealed a rather persistent north-westerly gradient with an amplitude varying between 0 and 0.14 $gm^{-3}km^{-1}$. This amplitude exhibited distinct maxima that coincide with significant changes of A_0 and L respectively.

The consistency of results derived by fitting the full volume and single zenith angles indicates that it might be advantageous to reduce the scan pattern to one or two zenith angles. This would reduce the scanning time to less than 100 seconds and therefore avoid jumps between the start and stop azimuth angle. In addition, this would allow a higher temporal resolution. Parameters A_0, h and L have been derived from five radiosonde launches carried out between 7 and 16 UTC. In a next step we plan to retrieve these parameters from ceilometer and MWR zenith observations to be independent from radiosonde observations and enabling operational application. In this respect we also want to investigate the applicability of the simple model for the vertical humidity profile for different weather situations and the impact of uncertainties in the parameters h and L. Further, we will investigate to what degree temporal change of IWV, gradient and wind speed are related.

For the frontal approach analyzed in this case study our retrieval can explain up to 88% of MWR slant path observations. The remaining deviations are due to structures with smaller scales than the linear gradient, as well as rapid changes of the water vapor field during single scans. It is highly plausible that these deviations can be attributed to convective plumes. In the future we plan to investigate more than one year of volume scan data in order to identify dominant patterns over long time scales. For linking the residuum to convective activity and land-surface processes, dedicated campaigns with a scanning water vapor DIAL are planned.

Acknowledgments

We gratefully acknowledge financial support by the SFB/TR 32 "Pattern in Soil-Vegetation-Atmosphere Systems: Monitoring, Modelling, and Data Assimilation" funded by the Deutsche Forschungsgemeinschaft (DFG). We thank the research center Jülich, especially Heiner Geiss and Birger Bohn from institute ICG-II who made the setup of the HATPRO instrument possible. MERIS retrievals were provided by FU Berlin.

References

[1] P. Albert, R. Bennartz, R. Preusker, R. Leinweber, and J. Fischer, "Remote sensing of atmospheric water vapor using the moderate resolution imaging sectrometer," *J. Atmos. Oceanic Technol.*, vol. 22, pp. 309–314, 2005.

[2] Wulfmeyer and . co authors, "The convective and orographically induced precipitation study (cops): The scientific strategy, the field phase, and first highlights." *Q. J. R. Meteorolog. Soc.*, submitted.

[3] J. Braun, C. Rocken, and J. Liljegren, "Comparisons of line-of-sight water vapor observations using the global positioning system and a pointing microwave radiometer," *J. Atmos. Oceanic Technol.*, vol. 20(5), pp. 606–612, 2003.

[4] S. Kneifel, S. Crewell, U. Löhnert, and J. Schween, "Investigating water vapor variability by groundbased microwave radiometry: evaluation using airborne observations," *IEEE Geosci. Remote Sens. Lett.*, vol. 6(1), pp. 157–161, 2009.

[5] S. Padmanabhan, C. Reising, S., J. Vivekanandan, and F. Iturbide-Sanchez, "Retrieval of atmospheric water vapor density with fine spatial resolution using three-dimensional tomographic inversion of microwave brightness temperatures measured by a network of scanning compact radiometers," *IEEE Trans. Geosci. Remote Sens.*, vol. 47(11), pp. 3708–3721, 2009.

[6] M. Schneebeli, "Advancements in ground-based microwave remote sensing of the troposphere - calibration, data retrieval and applications," Ph.D. dissertation, Universität Bern, Switzerland, 2009. [Online]. Available: http://www.iap.unibe.ch/publications/publication.php?type=PhdThesis&authorlike=schneebeli

[7] J. L. Davis, G. Elgered, A. E. Niell, and C. E. Kuehn, "Ground-based measurement of gradients in the 'wet' radio refractivity of air," *Radio Sci.*, vol. 28(6), pp. 1003–1018, 1993.

[8] P. Gradinarsky, L. and G. Elgered, "Horizontal gradients in the wet path delay derived from four years of microwave radiometer data," *Geophys. Res. Lett.*, vol. 27(16), pp. 2521–2524, 2000.

[9] T. Rose, S. Crewell, U. Löhnert, and C. Simmer, "A network suitable microwave radiometer for operational monitoring of the cloudy atmosphere," *Atmos. Res.*, vol. 75(3), pp. 183–200, 2005.

[10] S. Crewell and U. Löhnert, "Accuracy of boundary layer temperature profiles retrieved with multi-frequency, multi-angle microwave radiometry," *IEEE Trans. Geosci. Remote Sens.*, vol. 45(7), pp. 2195–2201, 2007.